



**HAL**  
open science

## Difference in the GPS deformation pattern of North and Central Zagros (Iran)

Andrea Walpersdorf, Denis Hatzfeld, H. Nankali, Farokh Tavakoli, F. Nilforoushan, M. Tatar, P. Vernant, J. Chery, F. Masson

► **To cite this version:**

Andrea Walpersdorf, Denis Hatzfeld, H. Nankali, Farokh Tavakoli, F. Nilforoushan, et al.. Difference in the GPS deformation pattern of North and Central Zagros (Iran). *Geophysical Journal International*, 2006, 167 (3), pp.1077-1088. 10.1111/j.1365-246X.2006.03147.x . insu-00270320

**HAL Id: insu-00270320**

**<https://insu.hal.science/insu-00270320>**

Submitted on 10 Mar 2021

**HAL** is a multi-disciplinary open access archive for the deposit and dissemination of scientific research documents, whether they are published or not. The documents may come from teaching and research institutions in France or abroad, or from public or private research centers.

L'archive ouverte pluridisciplinaire **HAL**, est destinée au dépôt et à la diffusion de documents scientifiques de niveau recherche, publiés ou non, émanant des établissements d'enseignement et de recherche français ou étrangers, des laboratoires publics ou privés.

# Difference in the GPS deformation pattern of North and Central Zagros (Iran)

A. Walpersdorf,<sup>1,\*</sup> D. Hatzfeld,<sup>1</sup> H. Nankali,<sup>3</sup> F. Tavakoli,<sup>3</sup> F. Nilforoushan,<sup>3</sup> M. Tatar,<sup>4</sup> P. Vernant,<sup>2</sup> J. Chéry<sup>2</sup> and F. Masson<sup>2</sup>

<sup>1</sup>Laboratoire de Géophysique Interne et Tectonophysique, Grenoble, France

<sup>2</sup>Laboratoire de Dynamique de la Lithosphère, Montpellier, France

<sup>3</sup>National Cartographic Center, Research Department, Tehran, Iran

<sup>4</sup>International Institute for Earthquake Engineering and Seismology, Tehran, Iran

Accepted 2006 July 17. Received 2006 July 7; in original form 2005 July 19

## SUMMARY

Measurements on either side of the Kazerun fault system in the Zagros Mountain Belt, Iran, show that the accommodation of the convergence of the Arabian and Eurasian Plates differs across the region. In northwest Zagros, the deformation is partitioned as 3–6 mm yr<sup>-1</sup> of shortening perpendicular to the axis of the mountain belt, and 4–6 mm yr<sup>-1</sup> of dextral strike-slip motion on northwest–southeast trending faults. No individual strike-slip fault seems to slip at a rate higher than ~2 mm yr<sup>-1</sup>. In southeast Zagros, the deformation is pure shortening of  $8 \pm 2$  mm yr<sup>-1</sup> occurring perpendicular to the simple folded belt and restricted to the Persian Gulf shore. The fact that most of the deformation is located in front of the simple folded belt, close to the Persian Gulf, while seismicity is more widely spread across the mountain belt, confirms the decoupling of the surface sedimentary layers from the seismogenic basement. A comparison with the folding and topography corroborates a southwestward propagation of the surface deformation. The difference in deformation between the two regions suggests that right-lateral shear cumulates on the north–south trending Kazerun strike-slip fault system to  $6 \pm 2$  mm yr<sup>-1</sup>.

**Key words:** continental deformation, fault motion, Global Positioning System (GPS), plate convergence, Satellite geodesy, Zagros.

## INTRODUCTION

The aim of our GPS surveys is to study (1) the location of superficial deformation in a sedimentary cover decoupled from the basement (case of southeastern Zagros) and (2) the different behaviour of deformation between southeastern and northwestern Zagros. This study will help to answer the following questions: Is the Zagros deformation field distributed or localized on individual faults? Is the transition between pure and oblique shortening, from southeastern to northwestern Zagros, visible in the present-day deformation field? Is there any evidence for strain partitioning in northwestern Zagros? How do the shallow sediments accommodate the present-day deformation and how does this superficial deformation compare with the basement deformation as evidenced by the seismicity?

The tectonic settings of the Zagros are given by the Eurasia–Arabia collision, taking place entirely inside Iran's political bor-

ders. The current Eurasia–Arabia convergence rate is estimated to increase from west to east along the Iranian Persian Gulf line from 18 to 25 mm yr<sup>-1</sup> oriented about 10°N (Fig. 1). This increase is due to the proximity of the Arabia–Eurasia Euler pole situated in North Africa at  $27.9 \pm 0.5^\circ\text{N}$ ,  $19.5 \pm 1.4^\circ\text{E}$  with  $0.41 \pm 0.01^\circ\text{Myr}^{-1}$  (Vernant *et al.* 2004, corroborating Euler pole locations of Sella *et al.* 2002; McClusky *et al.* 2000, 2003). The shortening is concentrated on the Iranian territory mainly across two mountain ranges, the Alborz in the north, the Zagros in the south, but slip on several important strike-slip faults that bound non-deforming blocks (e.g. Central Iran, Lut) also accommodate some shortening. At the southeastern margin of the Arabia–Eurasia collision zone, along the Makran, the shortening is absorbed by subduction of oceanic lithosphere beneath southeast Iran at 19.5 mm yr<sup>-1</sup> (Vernant *et al.* 2004). In the Persian Gulf, no shortening is observed (Tatar *et al.* 2002). The first GPS results indicated that the southeastern Zagros undergoes about 10 mm yr<sup>-1</sup> of pure shortening (Tatar *et al.* 2002).

The Zagros mountain belt is approximately 1500 km long, 250–400 km wide, and runs from eastern Turkey, where it connects to the North and East Anatolian faults, to the Oman Gulf, where it dies out at the Makran subduction zone (Fig. 1). The belt lies on

\*Corresponding author: LGIT, Maison des Géosciences, BP 53, 38041 Grenoble Cedex 9, France. E-mail: andrea.walpersdorf@obs.ujf-grenoble.fr.

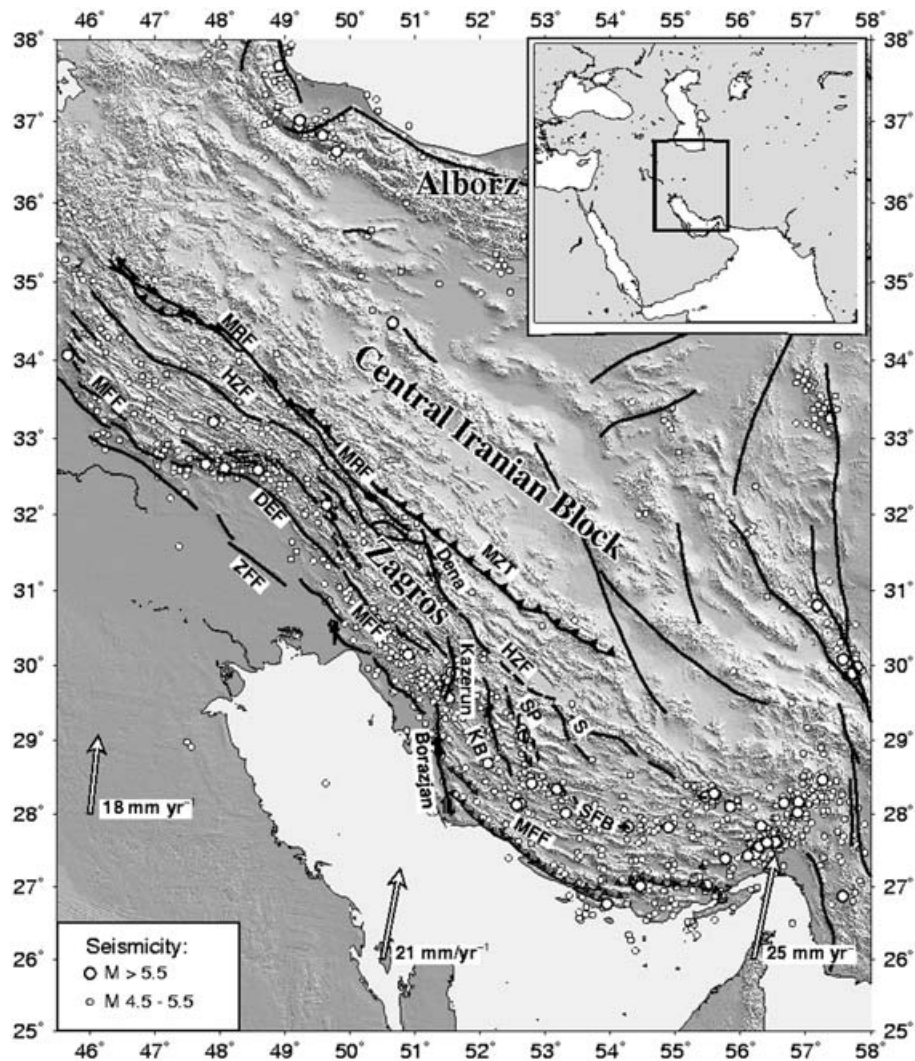


**Figure 1.** Location of the Zagros major active faults (Berberian 1995) and seismicity (Engdahl *et al.* 1998). The inset displays the global location of Zagros and Iran in the collision zone between the Arabian and Eurasian plates. The velocity vectors indicate the Arabia–Eurasia collision rate according to the rotation pole of Vernant *et al.* (2004). Zagros active faults are reported: MRF: Main Recent Fault; MZT: Main Zagros Thrust; HZF: High Zagros Fault; DEF: Dezful Embayment Fault; MFF: Zagros Mountain Front Fault; ZFF: Zagros Fore deep Fault; Dena fault; Kazerun fault; Borazjan fault; KB: Karez Bas fault; SP: Sabz Pushan fault; S: Sarvestan fault and SFB: simple fold belt (Berberian 1995).

the former Arabian passive margin that is covered by up to 10 km of Infracambrian to Miocene sediments (e.g. Haynes & McQuillan 1974; Stocklin 1974; Stoneley 1981). These sediments contain several layers of evaporite at different depths that decouple the surface deformation from the basement (Berberian 1981, 1995; Berberian & King 1981). During the Mesozoic, the Zagros underwent a major episode of convergence, mostly accommodated by subduction on the Main Zagros Thrust (MZT) (Stocklin 1974; Stoneley 1981). After the closure of the oceanic basins, a second episode of deformation during the Neogene led to the folding that affected the simple folded belt located between the MZT and the Persian Gulf (Falcon 1974).

The Zagros mountains are affected by the active NS trending Kazerun fault that offsets the folds and the lower Miocene terranes. Maximum and minimum displacement rates on the fault have been inferred from these offsets by Berberian (1981, 1995) and Authemayou *et al.* (2005) to 15 and 4 mm yr<sup>-1</sup>, respectively. Present-day activity of the Kazerun fault is evidenced by recent earthquakes with right lateral mechanisms located on the fault (Baker *et al.* 1993). The

main recent fault (MRF) is an active NW–SE trending right lateral strike-slip fault which runs along the MZT (Berberian 1995) and is observed northwest of the Kazerun fault (Tchalenko & Braud 1974; Ricou *et al.* 1977). The Dorud segment of the MRF is seismically the most active (Tchalenko & Braud 1974; Berberian 1981). A remarkable feature of the Zagros fold belt is that it propagates with time from the MZT towards the Persian Gulf (Falcon 1974; Shearman 1976; Berberian 1995; Hessami *et al.* 2001).

Most of the Zagros deformation seems to be aseismic (North 1974; Jackson *et al.* 1995; Masson *et al.* 2005). The seismicity is located in the basement, probably on reactivated former normal faults, and seems to be concentrated in the west of the mountain belt, in a region with a topography lower than 1000 m (Talebian & Jackson 2004).

Salt layers, present particularly in the southeastern part of Zagros, are suspected to create decoupling of the superficial layers from the basement. If this is the case, the Zagros deformation, as observed by GPS in the southeastern part, represents only the deformation of the sedimentary cover placed on top of the Arabian platform.

Talebian & Jackson (2004) proposed a kinematical description for the present-day deformation of the Zagros mountain belt. The authors compiled earthquake slip vectors related to thrust and strike-slip events and compare them with respect to the overall constraints given by the NUVEL1-A (DeMets *et al.* 1994) or REVEL (Sella *et al.* 2002) plate models. According to the present-day kinematics, the transition from pure shortening in southeast Zagros to oblique shortening in northwest Zagros is accommodated in the region of the Kazerun fault system.

## GPS DATA

We have measured two GPS networks in Zagros, the Central Zagros network covering the southeastern part, and the North Zagros network, covering the northwestern part (see site locations on Fig. 3). Data were collected in campaigns during 2001 and 2003 (18 forced antenna centring sites in North Zagros) and 1997, 2000 and 2003 (15 sites with tripod antenna set-up in Central Zagros) using a mixture of Trimble SSI and Ashtech Z-12 receivers and choke ring antennae. Each site was observed for at least 48 hr per campaign. During each campaign, we measured simultaneously some sites from the Iran Global network (KHOS, KSHA for North Zagros, ALIS, ARDA, LAMB for Central Zagros) (Nilforoushan *et al.* 2003; Vernant *et al.* 2004) to connect the different networks. Data from three Iranian permanent stations (AHVA, MASH, TEHR) were used in the campaign analyses when available. We also include the analysis of the GPS measurements (1999 and 2001) from the Iran Global network (Nilforoushan *et al.* 2003; Vernant *et al.* 2004) in the present study.

The data have been analysed with the GAMIT/GLOBK 10.1 software (King & Bock 2002). 32 IGS stations have been included to establish the terrestrial reference frame. Final IGS orbits and corresponding Earth orientation parameters have been used. In the combination of daily solutions with the Kalman filter GLOBK, the continuous time-series of daily SOPAC global solution files (IGS3 network) has been included from 1997 December to 2003 November, covering all measurement epochs presented here.

The precision of the inferred site velocities has been evaluated by (1) the campaign repeatabilities, giving the short term scatter of the site coordinate estimates and (2) velocity residuals on locally inferred rigid tectonic blocks, evaluating long-term uncertainties for the campaign stations (McClusky *et al.* 2000).

The average campaign repeatabilities are given in Table 1. They correspond to the increasing quality of the Central Zagros measurements (longer observation spans and more simultaneous observations by higher number of field teams). For the Central Zagros network, with a mean repeatability of 4 and 1 mm in 1997 and

**Table 1.** Mean repeatabilities on the north, east and vertical baseline components in each of the five campaigns presented in this paper. This statistic is limited on the local North Zagros and Central Zagros network stations with maximum baseline lengths of 3000 km. #bl is the number of measured baselines entering in the statistics.

| Repeatabilities [mm]: |          |     |     |     |     |
|-----------------------|----------|-----|-----|-----|-----|
| Campaign              | Epoch    | #bl | N   | E   | U   |
| C. Zagros             | 1997.918 | 25  | 2.8 | 3.0 | 7.4 |
| C. Zagros             | 2000.096 | 144 | 1.7 | 2.0 | 5.2 |
| N. Zagros             | 2001.721 | 233 | 1.1 | 1.7 | 4.7 |
| N. Zagros             | 2003.690 | 231 | 0.7 | 1.5 | 3.2 |
| C. Zagros             | 2003.885 | 206 | 0.9 | 1.3 | 2.8 |

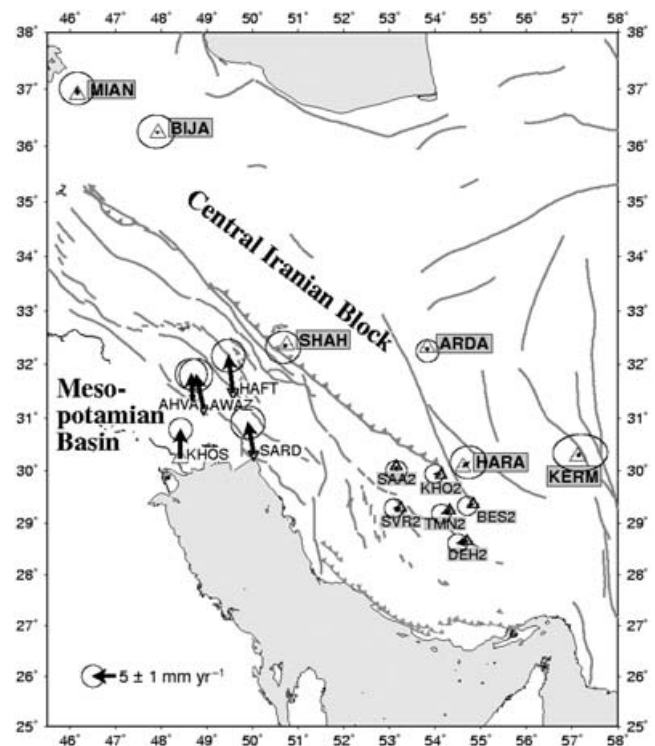


**Figure 2.** Identification of the two Iranian rigid blocks used for establishing the velocity precisions by evaluating the velocity residuals with respect to rigid block motion: the Central Iranian Block (stations MIAN, BIJA, SHAH, ARDA, HARA, KERM), which can be extended to the northern Central Zagros (stations SAA2, KHO2, SVR2, TMN2, DEH2, BER2), and the Mesopotamian basin (Stations AHVA, AWAZ, HAFT, KHOS, SARD).

2003, respectively, on the horizontal components, we could expect velocity uncertainties of  $1 \text{ mm yr}^{-1}$  over the 6 yr observation time span. Mean horizontal repeatabilities of 2 mm in the 2001 and 2003 North Zagros network yield a  $2 \text{ mm yr}^{-1}$  precision over the 2 yr time span.

Systematic errors like tripod set-up (in the Central Zagros network) or antenna phase centre offsets cannot be identified by the repeatability results only. These systematic errors do show up in the comparison of velocities for sites on the same tectonically rigid block. They contribute to the velocity residuals with respect to rigid block motion. Two rigid microblocks represented by several GPS sites can be used in this study to estimate velocity uncertainties (Fig. 2): The larger one is the Central Iranian block (stations MIAN, BIJA, SHAH, ARDA, HARA, KERM), the smaller one the Mesopotamian basin in the south of North Zagros (stations KHOS, AWAZ, AHVA, SARD, HAFT). We estimate horizontal residual velocities of  $1.9 \text{ mm yr}^{-1}$  on the Central Iranian block similar to Vernant *et al.* (2004). When we include six Central Zagros stations with low residual velocities with respect to Central Iran (SAA2, KHO2, BES2, SVR2, DEH2, TMN2; see Fig. 2), the average residuals with respect to a rigid motion of this block are evaluated to  $1.2 \text{ mm yr}^{-1}$ . In the Mesopotamian basin, south of North Zagros, the average residuals of the five site velocities KHOS, AWAZ, AHVA, SARD and HAFT are  $2.2 \text{ mm yr}^{-1}$ . These residuals with respect to a rigid block motion suggest that the uncertainty of the velocity estimates presented in this study is about  $2 \text{ mm yr}^{-1}$  with slightly smaller values for the Central Zagros measurements due to the 6 yr observation span, in spite of the tripod set-up in this network.

Therefore,  $2 \text{ mm yr}^{-1}$  seems to be a conservative value for the uncertainties in both the Central and the Northern Zagros. This value will be used as a lower bound on deformation estimates in the tectonic interpretation (see below).

## THE ZAGROS VELOCITY FIELD

To focus on the Zagros deformation, we define a reference frame by minimizing the velocities of the stations located on the Central Iranian block (MIAN, BIJA, SHAH, ARDA, HARA and KERM; see Fig. 2) following Vernant *et al.* (2004). The velocity field we obtain on the Zagros networks with respect to the Central Iran block is shown in Table 2 and Fig. 3(a). A general value for the uncertainty of our velocity estimates is  $2 \text{ mm yr}^{-1}$  as indicated above.

Along the Persian Gulf (stations KHOS, SARD, ALIS, KAN2, OSL2, BMG2, LAMB), velocities of  $6\text{--}10 \text{ mm yr}^{-1}$  are observed representing the eastward increasing motion of the Arabian plate relative to Central Iran. While the eastern site velocities are aligned with the BAHR (Bahrain) velocity vector, the more westerly stations show a rotation to NNW. The transition between pure shortening in the east and oblique shortening in the west is located near the right-lateral Kazerun fault system (Kazerun, Sabs Pushan, Kareh Bas and Sarvestan faults; see Fig. 1 for fault locations). A large northern region of Central Zagros does not deform relative to the Central Iranian block as demonstrated by the low residual velocities of the GPS sites SAA2, KHO2, SVR2, TMN2, BES2 and DEH2. This low deformation suggests that the MZT is inactive in this part of the Zagros and that the deformation in Central Zagros is concentrated further southwest, in the region close to the Persian Gulf shore. A more distributed velocity field is observed in North Zagros with velocities relative to Central Iran decreasing from  $6 \text{ mm yr}^{-1}$  at the coast to  $3 \text{ mm yr}^{-1}$  in the centre of the Zagros mountain belt and to zero on the northern side of the MRF.

The Zagros velocity field indicates relative displacement rates of the order of  $2 \text{ mm yr}^{-1}$  (at the limit of resolution) across several individual faults. In the North Zagros, we find this magnitude of strike-slip activity for the MRF and for the Dena fault, while for the Dezful embayment fault (DEF) and for the Zagros mountain front fault (MFF) the relative motion of  $2 \text{ mm yr}^{-1}$  is rather transpressive (for fault locations see Fig. 1). In the Central Zagros network,  $4\text{--}6 \text{ mm yr}^{-1}$  of shortening is restricted to the Zagros MFF. The difference in deformation between the two networks suggests  $3\text{--}6 \text{ mm yr}^{-1}$  of right lateral strike-slip motion on the NS trending Kazerun fault system, distributed over the Kazerun, Borazjan, Kareh Bas and Sabz Pushan faults.

The Zagros velocity field is also represented with respect to the Arabian plate as the larger tectonical unit bordering the Zagros deformation belt (Fig. 3b). The Arabian plate reference frame has been established by applying the Arabia–Eurasia rotation pole established by Vernant *et al.* (2004) ( $27.9^\circ\text{N}$ ,  $19.5^\circ\text{E}$ ,  $0.41^\circ \text{ Myr}^{-1}$ ), to the Zagros velocity field. The BAHR residual velocity is  $0.4 \text{ mm yr}^{-1}$ , and the residual velocities of the Iranian GPS sites along the Persian Gulf (AHVA, AWAZ, KHOS, SARD, ALIS, KAN2, OSL2, BMO2, LAMB) are evaluated to an average of  $2.9 \text{ mm yr}^{-1}$  mainly oriented W to WNW with larger values in the centre. The absence of velocity components parallel to the Arabia–Eurasia shortening axis and the velocity amplitudes hardly above the error limit of  $2 \text{ mm yr}^{-1}$  confirm the absence of shortening in the Persian Gulf.

The velocity field of northern Zagros has been estimated from only two measurements over a 2 yr time span. Therefore, it is probably unreliable to analyse pairs of site velocities to quantify precisely

the low (typically  $2 \text{ mm yr}^{-1}$ ) displacement rates along individual faults. However, the analysis of subsets of site velocities (e.g. velocities along transects as shown in the next section) and of strain calculated over the whole velocity field or a subset of stations (as shown later) can be used to average the individual velocity observations and obtain a more significant characterization and quantification of the deformation in the Zagros networks.

The GPS site velocities are interpreted in this paper as constant, interseismic displacement rates. This supposes that no coseismic instantaneous displacement is contained in the displacement rates of the GPS stations, due to earthquakes occurring close to the GPS stations in the time interval covered by the successive measurement campaigns. Seismic catalogues show that no significant earthquake ( $M_s > 6$ ) took place close to the stations in our network in the time between the surveys.

To infer fault slip velocities from GPS displacement rates, a deformation model would be necessary, taking into account the fault placements with respect to the GPS sites and the fault mechanisms. Both fault locations and motions are still poorly known for the Zagros, because most of the faults are blind faults (Berberian, 1995), so that in this work we restrict ourselves not to overinterpret single site velocities.

## COMPARISON OF THE DEFORMATION BETWEEN CENTRAL ZAGROS AND NORTH ZAGROS

The difference in deformation between Northern and Central Zagros can be highlighted by plotting the velocity distributions on transects (TN1, TN2, TN3 in the North Zagros, TC1 and TC2 in Central Zagros) perpendicular to the Zagros mountain belt (Fig. 4). We project the velocity of the closest stations onto directions parallel and perpendicular to the mountain axis and interpret these two directions as strike-slip and shortening components of active structures parallel to the Zagros mountain axis, with respect to Central Iran. The two velocity components are plotted with respect to the distance between the GPS site and the approximate emplacement of the MRF (Fig. 4).

In order to illustrate (but not to compute) the deformation patterns, we superpose simple mechanical models on top of the velocity observations. For the strike-slip component, we use a model of a locked strike-slip fault in an elastic half-space (Savage & Burford 1973) centred on the MRF or the MZT. This model is evaluated for a locking depth at 10 km. Note that the locking depth is not significant for describing the velocity distribution on the spatial scale of the transects.

In the North Zagros, for TN1 and TN2, located north, most of the strike-slip deformation is associated with the MRF, whereas for TN3, located further south, most of the strike-slip deformation is associated with the Zagros MFF. In the Central Zagros, the strike-slip component is approximately  $2 \text{ mm yr}^{-1}$  and it is located in the southwestern part of the network, near the Persian Gulf. There is a marked difference between the two parts of Zagros because the total strike-slip velocities vary from  $2 \text{ mm yr}^{-1}$  in Central Zagros to  $4\text{--}6 \text{ mm yr}^{-1}$  in North Zagros.

For the compressive component we use a model with a uniformly distributed homogeneous strain over the whole Zagros, corresponding to a linear velocity distribution. This simple model is sufficient to analyse the shortening patterns related to the young continental collision taking place throughout the Zagros. In this case of shortening, we fit the model to the velocity observations. While in North Zagros the ensemble of site velocities fit a linear velocity

**Table 2.** GPS velocity field with respect to the Central Iranian Block (CIB) and with respect to ITRF 2000. Networks: IG: Iran Global; NZ: North Zagros; CZ: Central Zagros; IP: Iran permanent; IGS: International GPS Service.

| GPS station velocities [mm yr <sup>-1</sup> ] |           |          |                                      |         |                     |         |   |             |  |
|---|-----------|----------|--------------------------------------|---------|---------------------|---------|---|-------------|--|
| SITE (net)                                    | Positions |          | Velocities w.r.t. Iran Central Block |         | ITRF2000 velocities |         | Velocity uncertainties (95 per cent conf. interval) |             |  |
|   | long (°E) | lat (°N) | v east                               | v north | v east              | v north | sig v east  | sig v north |  |
| MIAN (IG)                                     | 46.162    | 36.908   | -0.06                                | 1.34    | 23.87               | 23.55   | 1.59  | 1.46        |  |
| ILAM (IG)                                     | 46.427    | 33.648   | -0.65                                | 3.98    | 24.14               | 26.11   | 1.61  | 1.47        |  |
| DELO (NZ)                                     | 47.429    | 32.692   | 0.02                                 | 3.31    | 25.26               | 25.44   | 1.53  | 1.51        |  |
| GORI (NZ)                                     | 47.739    | 33.057   | -2.05                                | 3.75    | 23.15               | 25.93   | 1.51  | 1.49        |  |
| BIJA (IG)                                     | 47.930    | 36.232   | -0.46                                | 0.24    | 24.02               | 22.39   | 1.66  | 1.50        |  |
| KORA (NZ)                                     | 48.175    | 33.406   | 0.70                                 | 3.44    | 25.91               | 25.57   | 1.50  | 1.48        |  |
| KHOS (IG)                                     | 48.409    | 30.246   | 0.14                                 | 6.27    | 26.16               | 28.32   | 1.06  | 1.02        |  |
| BORU (NZ)                                     | 48.506    | 33.772   | -2.89                                | 1.05    | 22.32               | 23.13   | 1.50  | 1.48        |  |
| DEZF (NZ)                                     | 48.678    | 32.657   | -2.45                                | 4.58    | 23.06               | 26.66   | 1.50  | 1.48        |  |
| AHVA (IP)                                     | 48.684    | 31.340   | -0.29                                | 5.56    | 25.57               | 27.64   | 1.42  | 1.41        |  |
| AWAZ (NZ)                                     | 48.925    | 31.188   | -1.66                                | 7.12    | 24.23               | 29.25   | 1.50  | 1.48        |  |
| JOZA (NZ)                                     | 48.952    | 34.256   | -1.84                                | 2.71    | 23.36               | 24.77   | 1.50  | 1.48        |  |
| SOLE (NZ)                                     | 49.328    | 32.037   | -2.19                                | 4.71    | 23.62               | 26.84   | 1.50  | 1.48        |  |
| HAFT (NZ)                                     | 49.571    | 31.484   | -1.02                                | 7.96    | 24.97               | 29.96   | 1.50  | 1.48        |  |
| SHOL (NZ)                                     | 49.668    | 33.073   | 0.40                                 | 0.72    | 26.10               | 22.75   | 1.51  | 1.49        |  |
| GHAR (NZ)                                     | 49.851    | 35.140   | -0.26                                | 0.28    | 24.88               | 22.34   | 1.51  | 1.49        |  |
| SARD (NZ)                                     | 50.026    | 30.325   | -1.32                                | 6.88    | 24.93               | 28.88   | 1.52  | 1.49        |  |
| CHEL (NZ)                                     | 50.098    | 32.482   | -2.80                                | 3.75    | 23.12               | 25.81   | 1.51  | 1.49        |  |
| KHON (NZ)                                     | 50.458    | 33.157   | -1.82                                | -0.06   | 23.96               | 21.99   | 1.51  | 1.49        |  |
| KRD2 (NZ)                                     | 50.531    | 31.808   | -3.25                                | 1.71    | 22.80               | 23.76   | 1.50  | 1.48        |  |
| DEDA (NZ)                                     | 50.578    | 30.990   | 1.05                                 | 3.85    | 27.31               | 25.63   | 1.51  | 1.48        |  |
| BAHR (IGS)                                    | 50.608    | 26.209   | 4.83                                 | 6.74    | 31.99               | 28.76   | 0.52  | 0.23        |  |
| SHAH (IG)                                     | 50.748    | 32.367   | -0.79                                | -0.56   | 25.22               | 21.44   | 1.56  | 1.45        |  |
| ALIS (IG)                                     | 51.082    | 28.919   | -0.87                                | 8.17    | 25.92               | 30.13   | 1.04  | 1.00        |  |
| KSHA (IG)                                     | 51.255    | 34.150   | 0.21                                 | -0.60   | 25.94               | 21.34   | 1.05  | 1.02        |  |
| TEHN (IP)                                     | 51.334    | 35.697   | -0.78                                | -3.02   | 24.59               | 18.94   | 1.39  | 1.38        |  |
| TEHR (IG)                                     | 51.386    | 35.747   | 0.81                                 | -1.27   | 26.16               | 20.68   | 1.65  | 1.51        |  |
| SEMI (NZ)                                     | 51.430    | 31.225   | -2.93                                | 0.19    | 23.40               | 22.21   | 1.51  | 1.49        |  |
| NOSH (IG)                                     | 51.768    | 36.586   | -2.10                                | -3.09   | 23.17               | 18.79   | 1.71  | 1.50        |  |
| QOMS (IG)                                     | 51.799    | 32.250   | -1.90                                | 0.75    | 24.32               | 22.67   | 1.51  | 1.48        |  |
| KAN2 (CZ)                                     | 52.056    | 27.834   | 0.87                                 | 8.10    | 28.01               | 30.03   | 0.88  | 0.86        |  |
| FAR2 (CZ)                                     | 52.106    | 28.851   | -1.88                                | 5.32    | 25.08               | 27.19   | 0.88  | 0.85        |  |
| OSL2 (CZ)                                     | 52.607    | 27.474   | 0.11                                 | 9.16    | 27.36               | 30.98   | 1.63  | 1.52        |  |
| QIR2 (CZ)                                     | 53.029    | 28.477   | -2.08                                | 1.53    | 25.11               | 23.38   | 0.84  | 0.83        |  |
| ISL2 (CZ)                                     | 53.066    | 28.347   | -1.42                                | 2.60    | 25.87               | 24.40   | 0.86  | 0.84        |  |
| SAA2 (CZ)                                     | 53.146    | 30.087   | 0.03                                 | -0.92   | 27.03               | 20.92   | 0.95  | 0.88        |  |
| SVR2 (CZ)                                     | 53.244    | 29.281   | -1.48                                | 0.04    | 25.63               | 21.94   | 0.88  | 0.85        |  |
| BMG2 (CZ)                                     | 53.480    | 26.970   | 3.15                                 | 5.81    | 30.67               | 28.35   | 1.08  | 1.08        |  |
| SEMN (IG)                                     | 53.564    | 35.662   | 0.15                                 | -5.82   | 26.07               | 15.94   | 1.64  | 1.48        |  |
| GOT2 (CZ)                                     | 53.631    | 28.624   | -0.70                                | 2.42    | 26.57               | 24.23   | 0.99  | 0.95        |  |
| BIG2 (CZ)                                     | 53.637    | 27.852   | -0.56                                | 1.52    | 26.81               | 23.37   | 0.92  | 0.90        |  |
| ARDA (IG)                                     | 53.822    | 32.313   | 0.10                                 | -0.75   | 26.78               | 21.02   | 1.02  | 1.00        |  |
| LAMB (IG)                                     | 54.004    | 26.883   | 3.50                                 | 7.22    | 31.14               | 28.92   | 1.08  | 1.01        |  |
| KHO2 (CZ)                                     | 54.126    | 29.923   | -1.42                                | 0.24    | 25.70               | 22.02   | 0.86  | 0.85        |  |
| KORD (IG)                                     | 54.199    | 36.860   | -0.78                                | -9.41   | 24.94               | 12.04   | 1.67  | 1.49        |  |
| TMN2 (CZ)                                     | 54.316    | 29.239   | -1.85                                | -0.67   | 25.44               | 21.06   | 0.86  | 0.85        |  |
| LAR2 (CZ)                                     | 54.320    | 27.644   | 0.59                                 | 4.33    | 28.16               | 26.07   | 0.89  | 0.86        |  |
| HARA (IG)                                     | 54.608    | 30.079   | 1.20                                 | 0.99    | 28.41               | 22.71   | 1.63  | 1.47        |  |
| DEH2 (CZ)                                     | 54.700    | 28.645   | -2.15                                | -0.44   | 25.34               | 21.31   | 0.87  | 0.85        |  |
| BES2 (CZ)                                     | 54.832    | 29.363   | -1.32                                | -0.40   | 26.08               | 21.32   | 0.87  | 0.85        |  |
| ROBA (IG)                                     | 56.070    | 33.369   | 1.56                                 | -4.11   | 28.45               | 17.48   | 1.60  | 1.46        |  |
| KHAS (IG)                                     | 56.233    | 26.208   | 3.32                                 | 9.79    | 31.43               | 31.31   | 1.83  | 1.50        |  |
| KERM (IG)                                     | 57.119    | 30.277   | 0.56                                 | 0.79    | 28.22               | 22.25   | 2.45  | 1.66        |  |

distribution along the transects (and therefore a homogeneous strain), in Central Zagros the velocity gradients are constrained excluding the stations in the non-deformable part of Central Iran. We observe an increase of the shortening component from North Zagros to Central Zagros (from 2 mm yr<sup>-1</sup> to 8 mm yr<sup>-1</sup>) due to the

proximity of the relative Arabia–Eurasia rotation pole (e.g. Sella *et al.* 2002; Vernant *et al.* 2004).

With an uncertainty of 2 mm yr<sup>-1</sup> on our velocity estimates (not including the systematic bias that are not measurable before a third campaign), we will only provide a first-order interpretation of the

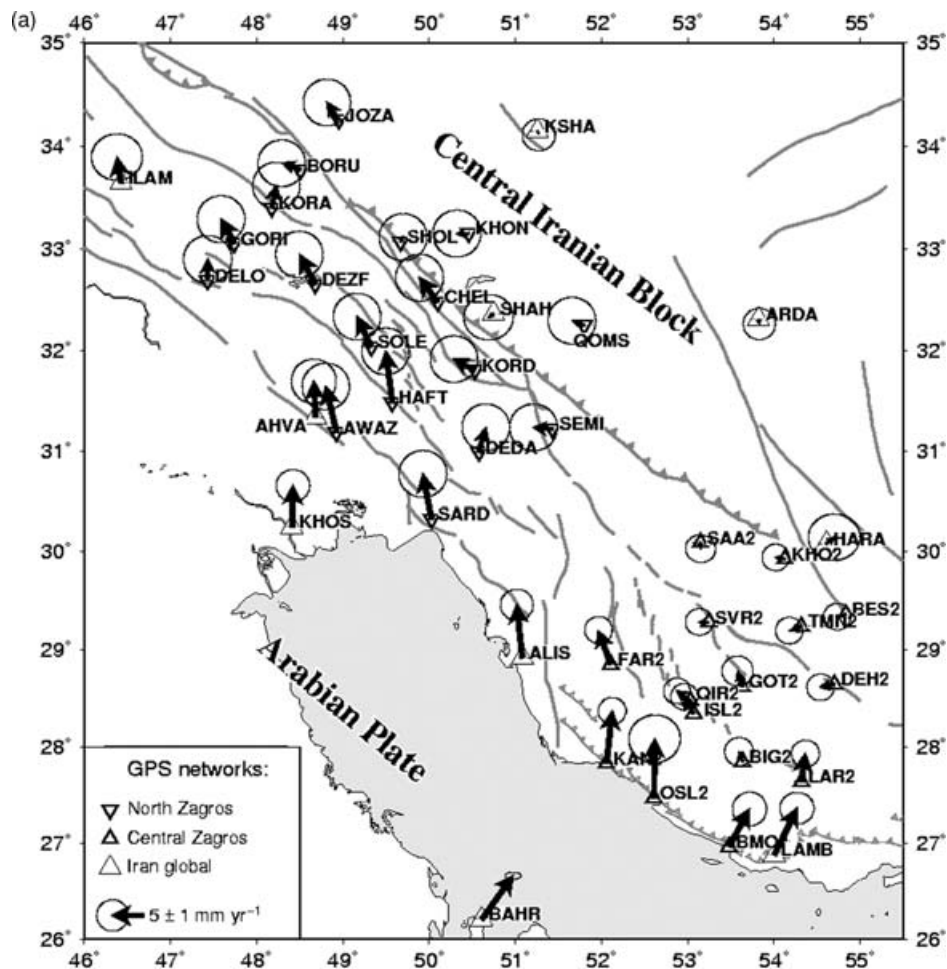


**Figure 3.** (a) North Zagros and Central Zagros velocity fields with respect to the Central Iranian block. The scale vector corresponds to  $5 \text{ mm yr}^{-1}$ . The error ellipses indicate formal errors within a 95 per cent confidence interval. The different networks (North Zagros, Central Zagros and Iran Global) are marked with different symbols. We observe a different velocity field on both sides of the Kazerun fault system. (b) North Zagros and Central Zagros velocity fields with respect to the Arabian Plate. Same captions as Fig. 3(a).

tectonics of the region and not try to estimate the strike-slip rates on individual faults of the Zagros folded belt (MRF, High Zagros Fault, Zagros MFF). The fault parallel component (strike-slip motion) in North Zagros increases from north to south (from transect TN1 to TN3) from 4 to  $6 \text{ mm yr}^{-1}$ . This strike-slip motion is observed along transect TN1 for the stations located on the Zagros folded belt (DELO–ILAM–GORI–DEZF–KORA–BORU) relative to Central Iran (GARA), on TN2 for the stations located south of the Dezful Embayment (AWAZ–HAFT) relative to the Zagros folded belt (SOLE–KORD–CHEL) and Central Iran (SHOL–KHON), and along transect TN3 for the stations located south of the Zagros MFF (ALIS–SARD) relative to the Zagros folded belt (DEDA–SEMI) and Central Iran (QOMS–ARDA).

Shortening is insignificant in the region spanned by the transect TN1 (DELO–GORI–KORA–BORU–JOZA). Further south, on transect TN2, the stations south of the DEF (KHOS–AWAZ–HAFT) converge relative to the Zagros folded belt stations (SOLE–KORD–CHEL–SHOL–SHAH) with a velocity of about  $3 \pm 1 \text{ mm yr}^{-1}$ . On transect TN3, the NS trending Kazerun fault marks a place of several  $\text{mm yr}^{-1}$  of shortening due to its obliqueness with respect to the profile.

For the Central Zagros, a fault parallel motion of  $2 \pm 1 \text{ mm yr}^{-1}$  relative to Central Iran affects the westernmost stations (KAN2–

OSL2–FAR2) suggesting that a small amount of strike-slip motion (with respect to the orientation of the MRF/MZT) is accommodated by the Kazerun fault system. On the contrary, the shortening shows a large gradient of up to  $8 \text{ mm yr}^{-1}$  between stations located on the Persian Gulf shore (KAN2–OSL2 on TC1 and BMG2–LAMB on TC2) and all other stations located further north (SAA2–TMN2–KHO2–HARA on TC1 and DEH2–KERM on TC2). Only the two stations BIG2 and LAR2 located further inland show a slow convergence ( $3 \pm 1 \text{ mm yr}^{-1}$ ) toward Central Iran. This suggests that most of the shortening (75 per cent) is accommodated by structures located along the Persian Gulf such as the Zagros MFF.

### SLIP RATES FOR THE KAZERUN FAULT SYSTEM

As seen in Fig. 1, the Kazerun fault system separates the Zagros into two regions of contrasting deformation systems and, therefore, it should accommodate some differential motion. We can infer velocity estimates on different segments of the Kazerun fault system by comparing the velocity fields in the North and the Central Zagros on each side of the fault system.

The two stations located south of the Zagros MFF (KAN2 and ALIS) on either side of the fault system show similar motion relative

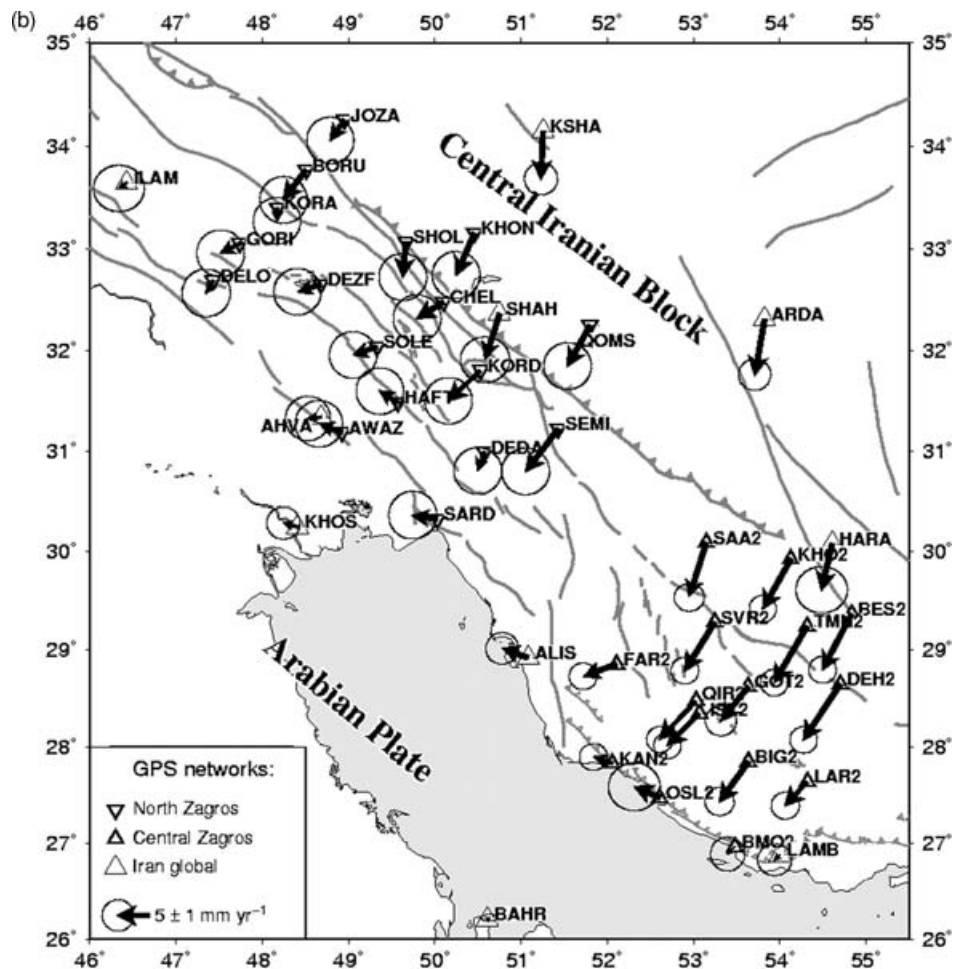


Figure 3. (Continued.)

to Central Iran, which suggests that they both belong to the non-deformable part of the Arabian plate. However, going further north, we measure  $3 \pm 2 \text{ mm yr}^{-1}$  of relative NS displacement between ALIS and FAR2, which characterizes the slip rate in the southern part of the Kazerun fault system. We also measure  $3 \pm 2 \text{ mm yr}^{-1}$  between DEDA and SEMI which can be attributed to the Dena fault. The motion on the Karebas and on the Sabz Pushan faults can be estimated from the comparison between FAR2 and QIR2 on one hand and FAR2 and SVR2 on the other hand, suggesting a motion of about  $2 \pm 2 \text{ mm yr}^{-1}$  of the Karebas fault and almost of the same order on Sabz Pushan. Therefore, the cumulated motion accommodated by the total Kazerun strike-slip fault system is of about  $6 \pm 2 \text{ mm yr}^{-1}$ .

### THE ZAGROS STRAIN DISTRIBUTION

The strain tensors obtained over 19 stations in the North Zagros and 15 stations in Central Zagros are shown in Fig. 5(a). Over the whole North Zagros network, we see a dominating compressive component oriented perpendicular to the mountain axis. A smaller extensive component is assumed to be due to a strike-slip component present in the overall deformation pattern. In Central Zagros, we notice higher strain rates (25 per cent) on both the compressive and the extensive component with respect to North Zagros. The decrease of the overall deformation rates from Central to North Zagros could be

due to two reasons: First, the North Zagros network is larger than the Central Zagros network, so that the velocity differences are spread over larger distances and second, the relative motion between Arabia and Eurasia decreases from east to west according to the Eurasia–Arabia rotation pole (Vernant *et al.* 2004).

In order to compare the distribution of the deformation in both the Northern and Central Zagros, we define several subnetworks (three in the southeast and five in the northwest) of similar sizes to compare strain rates (Fig. 5b). The numerical values are summarized in Table 3. The formal errors of the strain estimates are 10–15 nanostrain  $\text{yr}^{-1}$ . We conclude that significant deformation can be shown by the present analysis in subnetworks where values of more than 10–15 nanostrain  $\text{yr}^{-1}$  are obtained. The values observed for two subnetworks being situated in supposedly non-deforming parts of the network, NZ1 in the Mesopotamian basin in the North Zagros, and CZ1 in the northern part of Central Zagros, are of 5–10 nanostrain  $\text{yr}^{-1}$ . Based on significant strain observations, we note that the strain distribution is different in Central Zagros with respect to North Zagros. In Central Zagros, the compressional axes are parallel to each other and perpendicular to the fold axes and most of the deformation is concentrated in one band along the Persian Gulf coast, in CZ3. In North Zagros, the compressional axes vary in orientation, and two separate zones of significant deformation can be distinguished, NZ2, and NZ4a and NZ4b. This analysis of the strain rates in subnetworks shows that the deformation is not homogeneously distributed but concentrated in zones located near active

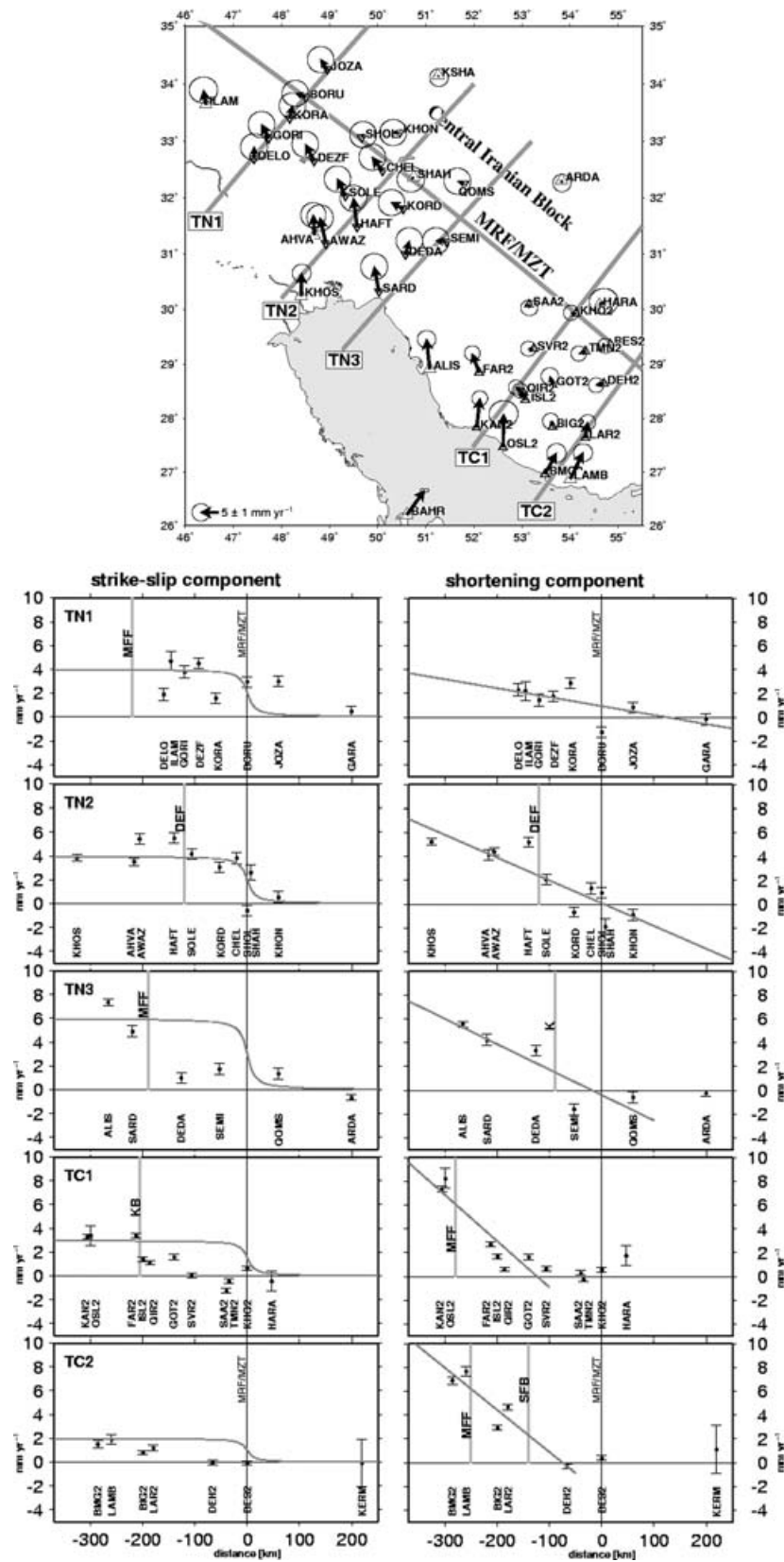


**Figure 4.** Site velocities ( $\text{mm yr}^{-1}$ ) with respect to the site distance to the main recent fault (MRF)/main Zagros thrust (MZT) (in km, on the  $x$ -axis) on 5 transects (locations shown on the map), TN1, TN2 and TN3 in the North Zagros, TC1 and TC2 in the Central Zagros, from northwest to southeast. On the left, we display the fault parallel components (strike-slip component), on the right, the fault perpendicular component (shortening). A simple model is superposed on the individual velocities (dark grey lines, for details see text). Modelled total strike-slip velocities vary from 2 to 6  $\text{mm yr}^{-1}$ , strain rates from 8 to 39 nanostrain  $\text{yr}^{-1}$ . Light grey vertical lines indicate fault locations.

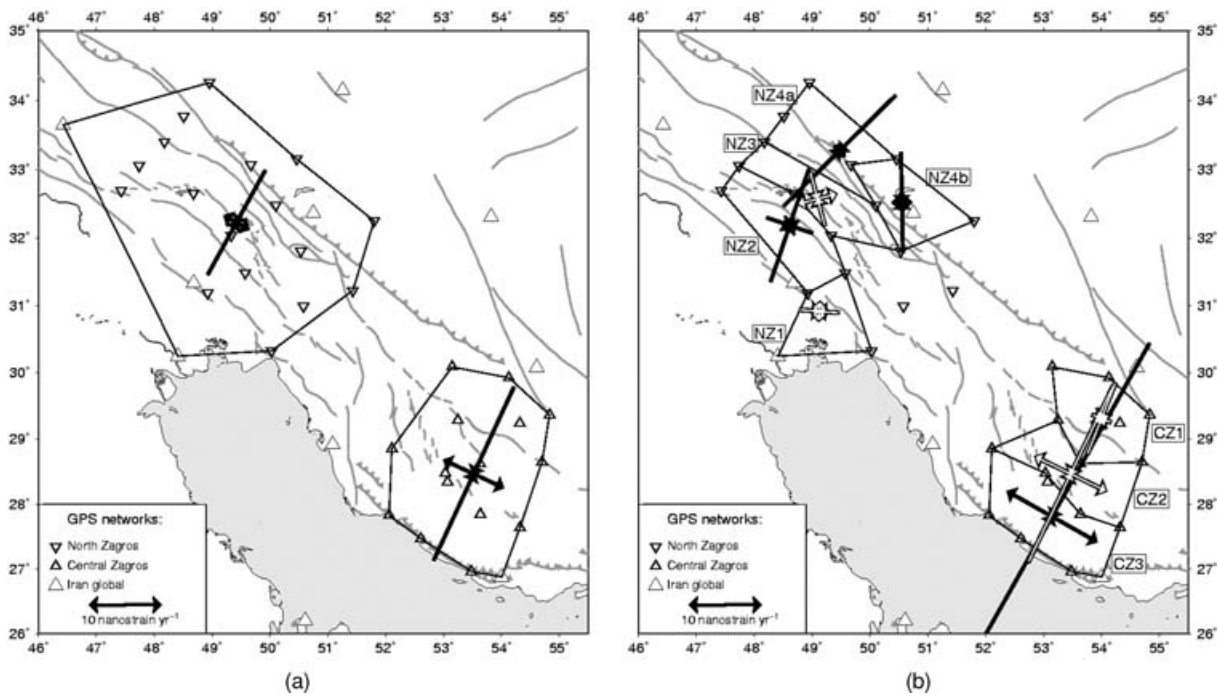


**Figure 5.** (a) Overall strain rates in the North and Central Zagros networks. Numerical values are indicated in Table 3. (b) Strain rates in subnetworks. Black and white strain crosses distinguish relatively high and low deformation rates, respectively.

**Table 3.** Strain rate values and their uncertainties for the main networks, for the five North Zagros subnetworks and the three Central Zagros subnetworks. The most significant values in the subnetworks are highlighted. For the localization of the subnetworks refer to Fig. 5(b).

| North and central Zagros strain rates in nanostrain yr <sup>-1</sup> |              |                                    |                                  |                |                                   |                                  |
|--|--------------|------------------------------------|----------------------------------|----------------|-----------------------------------|----------------------------------|
|  | North Zagros | Major axis                         | Sec. axis                        | Central Zagros | Major axis                        | Sec. axis                        |
| Main networks:   | NZ           | $-16.5 \pm 3.0$                    | $3.9 \pm 2.5$                    | CZ             | $-27.3 \pm 3.0$                   | $9.2 \pm 2.9$                    |
| Subnetworks:   | NZ1          | $-5.5 \pm 10.8$                    | $2.6 \pm 9.9$                    | CZ1            | $-10.7 \pm 6.8$                   | $-2.6 \pm 5.2$                   |
|  | <b>NZ2</b>   | <b><math>-16.9 \pm 14.9</math></b> | <b><math>-6.8 \pm 9.3</math></b> | CZ2            | $-23.4 \pm 1.2$                   | $11.1 \pm 3.8$                   |
|  | NZ3          | $-7.7 \pm 15.1$                    | $5.4 \pm 15.8$                   | <b>CZ3</b>     | <b><math>-57.0 \pm 7.4</math></b> | <b><math>14.6 \pm 3.7</math></b> |
|  | <b>NZ4a</b>  | <b><math>-22.5 \pm 14.3</math></b> | <b><math>2.0 \pm 7.8</math></b>  |                |                                   |                                  |
|  | <b>NZ4b</b>  | <b><math>-14.2 \pm 13.0</math></b> | <b><math>2.6 \pm 11.2</math></b> |                |                                   |                                  |

faults, such as the MFF (CZ3) in Central Zagros, and the DEF/MFF (NZ2) and the MRF (NZ4a/b) in North Zagros.

## COMPARISON WITH SEISMICITY

To compare the shallow deformation with the basement deformation, we have to compare the GPS results with seismicity. Two cross sections across the Zagros (Fig. 6) have been chosen to study the distribution of seismicity with respect to the Zagros topography and the GPS measured surface displacement rates. The topography shows that the width of the belt in North Zagros is much narrower than in Central Zagros (~200 versus ~350 km). However, the average altitude of the deforming belt (the simple fold belt) is lower in North Zagros (excluding Mt. Dena which is in a peculiar region) than in Central Zagros, while one expects that comparable deformation over a narrower range would lead to higher altitudes. One explanation for this difference is the additional strike-slip motion present in North Zagros while Central Zagros deformation is dominated by thrusting. This means that, contrary to the Central Zagros, the crust is not trapped in North Zagros but can escape from pure shortening (and therefore folding) by lateral translation along strike-slip faults such as the MRF. A second reason for the lower deformation in North

Zagros is the decrease of relative motion in the Arabia–Eurasia collision with respect to Central Zagros.

Talebian & Jackson (2004) showed that larger magnitude seismicity is restricted to the edge of the Zagros fold belt and, therefore, could be associated with only the most recent of the faults proposed by Berberian (1995) in the Zagros. This was even more apparent when considering only the earthquakes of magnitude  $M_b > 5$  that are located in regions of low topography. However, microearthquake seismicity is spread on a wider region (Tatar *et al.* 2004). We plotted both the total seismicity available in the ISC catalogue and the relocated earthquakes of magnitude  $m_b > 5$  (Engdahl *et al.* 1998) in Fig. 6. The superficial deformation of Central Zagros inferred from GPS measurements is much more concentrated along the Persian Gulf coast than shown by the seismicity (Fig. 6, TC1). Models of the Zagros folded deformation are derived from balanced cross sections of the sedimentary cover (i.e. McQuarrie 2004; Sherkaty & Letouzey 2004; Molinaro *et al.* 2005). These models assume that the sedimentary cover folds whereas the basement is affected by active faults. Some of the listed authors assume that every fold is related to an active fault. If the sedimentary cover is totally decoupled from the basement, then there is no need for the surface folds to be located at the same place as the active faults in the basement (Tatar

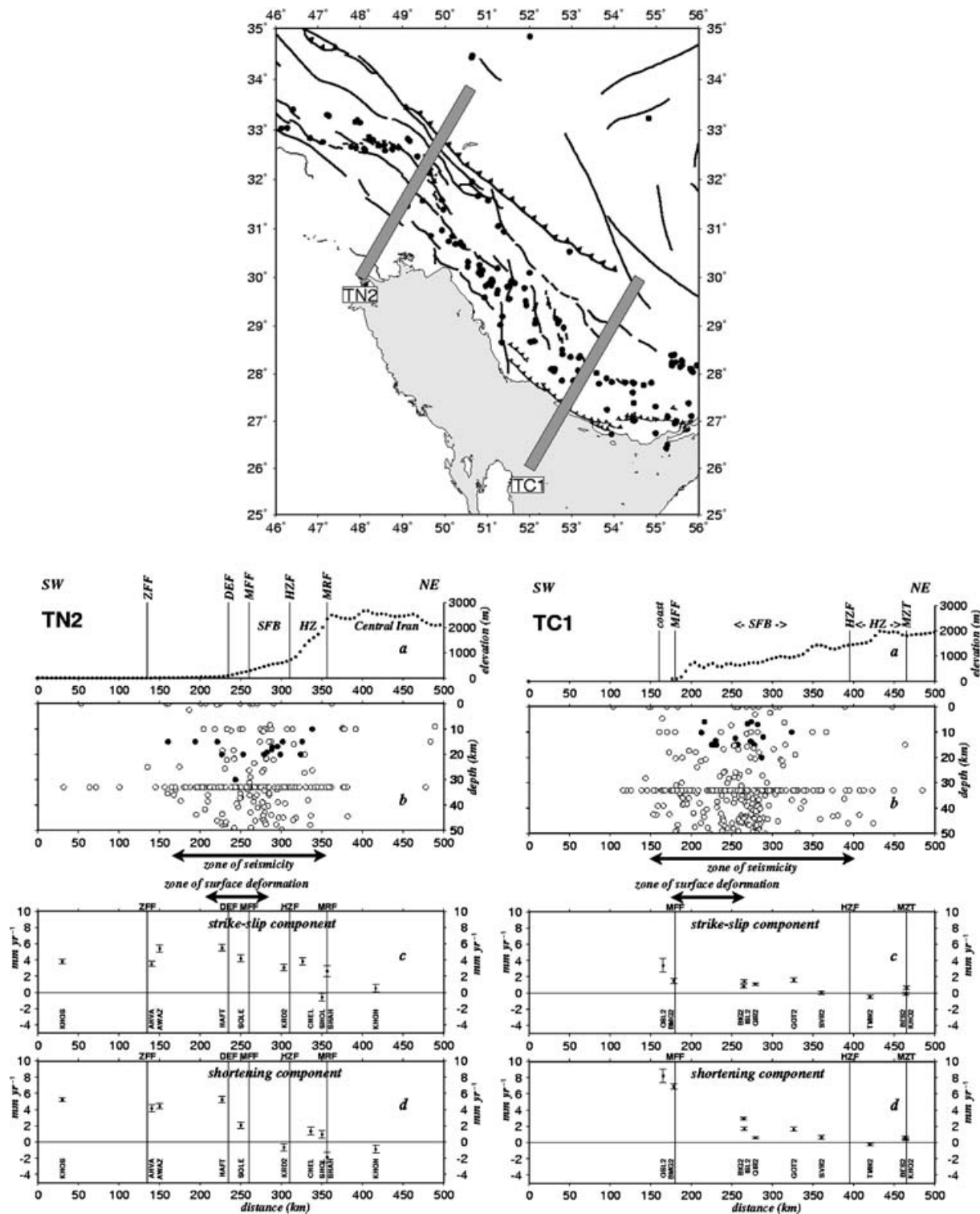


**Figure 6.** On the two transects TN2 and TC1 we display (a) the topography, (b) the seismicity (open circles: USGS, black circles: Engdahl *et al.* 1998), (c) NW–SE strike-slip motion parallel to MRF/MZT and (d) shortening perpendicular to MRF/MZT. The approximate location of different faults is indicated by vertical lines. Horizontal arrows indicate that the surface deformation evidenced by GPS measurement is concentrated in narrow areas, whereas the basement deformation evidenced by the seismicity is distributed in a larger area, suggesting a decoupling between the two.

*et al.* 2004). The only constraint is that both the deformation of the basement (seismicity) and of the shallow sedimentary cover (GPS) should be of comparable value. However, the comparison between the brittle deformation evidenced by earthquake activity and the

tal deformation inferred by strain from GPS measurements shows that only 10 per cent of the total deformation in Zagros is released by earthquakes (North 1974; Jackson & McKenzie 1988; Masson *et al.* 2005).

There are two possible explanations for the relatively aseismic deformation of the Zagros. Firstly, that the amount of deformation of the basement is smaller (by 80 per cent) than the deformation evidenced at surface by GPS. This implies that the Zagros basement underthrusts beneath the Central Iran region to the northeast, as an active subduction. This seems unlikely because we do not observe any seismicity located north of the MZT that acted as the suture of former subduction (Maggi *et al.* 2000; Talebian & Jackson 2004). Secondly, that the mechanical properties do not allow all the deformation to release seismic energy probably because of the unusually large thickness of the sedimentary cover that reduces the thickness of the brittle crust.

## CONCLUSIONS

The two GPS surveys in the North Zagros give a consistent velocity field relative to Central Iran. The third survey in Central Zagros increases the precision of the velocity field and allows a comparison with North Zagros. The average velocity uncertainties are evaluated to 2 mm yr<sup>-1</sup>.

Present-day deformation in the North Zagros is characterized by cumulated 3–6 mm yr<sup>-1</sup> of shortening and cumulated 4–6 mm yr<sup>-1</sup> of right-lateral strike-slip, consistent with first estimates from the larger scale Iran Global GPS network (Vernant *et al.* 2004). This strike-slip motion is lower than the 10–17 mm yr<sup>-1</sup> proposed on only the MRF by Talebian and Jackson (2002). Talebian and Jackson suggested this slip rate based on the assumption that the observed offset of 50 km on the MRF was achieved in 3–5 Ma. If we assume a constant slip rate of at most 4–6 mm yr<sup>-1</sup> (cumulated slip rate across the whole North Zagros mountain belt), the MRF has formed not earlier than 10 Ma ago. In our study, 2–3 mm yr<sup>-1</sup> of slip rate have been localized on the MRF, resulting in a fault age of 25 Ma. We can compare these estimates for the MRF with those of the Kazerun fault, as their respective onsets are certainly related. On the Kazerun fault, fault offsets between 12–27 km (minimal values, Authemayou *et al.* 2005) and 140 km (Berberian 1995) have been suggested. The GPS inferred present-day displacement rates we can take into account are 6 ± 2 mm yr<sup>-1</sup> (maximum value inferred across the whole Kazerun strike-slip fault system) and 2 mm yr<sup>-1</sup> (restricted to the Kazerun fault *sensu stricto*). Considering fault offsets of around 20 km, the latest onset time is about 3 Ma with a constant displacement rate of 6 ± 2 mm yr<sup>-1</sup>, the earliest onset time is about 10 Ma with a constant slip rate of 2 mm yr<sup>-1</sup>. These estimates are lower, but reaching the same order of magnitude as for the MRF. This could evidence a simultaneous onset of both faults. The Kazerun fault offset of 140 km as postulated by Berberian (1995) implies an earliest onset 35 Ma ago and does not seem to correspond to the same tectonical period.

In Central Zagros, 8 mm yr<sup>-1</sup> of shortening and 2–3 mm yr<sup>-1</sup> of strike-slip motion are observed, consistent with the first results of Tatar *et al.* (2002). This increase of the rate of shortening in Central Zagros compared to North Zagros is consistent with the location of the Arabia–Eurasia rotation pole which predicts an increase of 4 mm yr<sup>-1</sup> for the NS component between KHOS and LAMB. We confirm Tatar *et al.*'s (2002) result that the MZT is currently inactive but the Central Zagros velocity field is distributed differently than proposed by Tatar *et al.* (2002). The northern region not deforming relatively to the Central Iranian block is spread over a larger zone, and the shortening is more concentrated along the coast of the Persian Gulf. In both studies, a small strike-slip component is observed in the western part of the network near the Kazerun strike-slip

fault system, coherent to Talebian & Jackson's (2004) kinematical description.

The GPS measured deformation of Central Zagros concentrated along the coast is consistent with geomorphological observations (such as growth rates of folds evidenced by terrace uplifts, Vita-Finzi 1987; Oveisi, personal communication, 2005) and supports a model of propagation of the folding deformation to the SW (Shearman 1976; Hessami *et al.* 2001). The comparison between the superficial deformation concentrated along the coastline and the more widely spread seismicity confirms the decoupling of the sedimentary layer from the basement.

The North Zagros velocity field is more complex with the presence of shortening and strike-slip distributed across the belt. The strike-slip motion is likely associated with the MRF and shortening with the DEF but our data do not help to quantify this motion on single faults. No individual fault seems to present slip rates of more than 2 mm yr<sup>-1</sup>.

Therefore, the deformation occurring in the Central Zagros (pure shortening) is different from that in North Zagros (partitioned between shortening and strike-slip), as is suggested by tectonic and seismological observations (i.e. Ricou *et al.* 1977; Berberian 1995; Talebian & Jackson 2004; Authemayou *et al.* 2006) and the morphology. The two parts of the Zagros are separated by the Kazerun fault system across which right-lateral strike-slip occurs at ~2–3 mm yr<sup>-1</sup> on individual fault segments, yielding a cumulated strike-slip rate of 6 ± 2 mm yr<sup>-1</sup>.

## ACKNOWLEDGMENTS

The GPS campaigns have been successful thanks to the help of many colleagues: M. Peyret, M.-N. Bouin, C. Sue, and the field teams of NCC and IIEES in Tehran. This project was financed by the CNRS-INSU 'Intérieur de la Terre' programme, the NCC and the IIEES. HN, FN, MT and FT were partially supported by the French Embassy in Tehran. The GPS receivers were provided by CNRS-INSU and NCC. We benefited from interesting discussions with M. Berberian, J. Jackson, P. Molnar, M. Talebian, C. Vita-Finzi and P. Tregoning, and from a constructive review by V. Regard.

## REFERENCES

- Authemayou, C., Bellier, O., Chardon, D., Malekzade, Z. & Abassi, M., 2005. Role of the Kazerun fault system in active deformation of the Zagros fold-and-thrust belt (Iran), *Comptes Rendus Geoscience*, **337**(5), 475–547.
- Authemayou, C., Chardon, D., Bellier, O., Malekzade, Z., Shabanian, I. & Abbassi, M., 2006. Late Cenozoic Partitioning of oblique plate convergence in the Zagros fault-and-thrust belt (Iran), *Tectonics*, **25**, TC3002, doi:10.1029/2005TC001860, 2006.
- Baker, C., Jackson, J. & Priestley, K., 1993. Earthquakes on the Kazerun Line in the Zagros mountains of Iran: strike-slip faulting within a fold-and-thrust belt, *Geophys. J. Int.*, **115**, 41–61.
- Berberian, M., 1981. Active faulting and tectonics of Iran, in *Zagros-Hindu-Kush-Himalaya Geodynamic evolution*, Vol. 3, pp. 33–69, eds Gupta, H.K. & Delany, F.M., Am. Geophys. Union, Geodyn. Ser.
- Berberian, M., 1995. Master blind thrust faults hidden under the Zagros folds: active basement tectonics and surface morphotectonics, *Tectonophysics*, **241**, 193–224.
- Berberian, M. & King, G.C.P., 1981. Towards a paleogeography and tectonic evolution of Iran, *Can. J. Earth Sci.*, **18**, 210–265.
- DeMets, C., Gordon, R.G., Argus, D.F. & Stein, S., 1994. Effects of recent revisions to the geomagnetic reversal time scale on estimates of current plate motions, *Geophys. Res. Lett.*, **21**, 2191–2194.

- Engdahl, E.R., Van der Hilst, R.D. & Buland, R.P., 1998. Global teleseismic earthquake relocation with improved travel times and procedures for depth determination, *Bull. seism. Soc. Am.*, **88**, 722–743.
- Falcon, N., 1974. Southern Iran: Zagros Mountains, in *Mesozoic-Cenozoic Orogenic Belts*, Vol. 4, pp. 199–211, ed. Spencer, A.M, Spc. Publ. Geol. Soc. London.
- Haynes, S.J. & McQuillan, H., 1974. Evolution of the Zagros suture zone, southern Iran, *Bull. geol. Soc. Am.*, **85**, 739–744.
- Hessami, K., Koyi, H., Talbot, C.J., Tabasi, H. & Shabanian, E., 2001. Progressive unconformities within and evolving foreland fold-thrust belt, Zagros Mountains, *J. geol. Soc. Lond.*, **158**, 969–981.
- Jackson, J. & McKenzie, D., 1988. The relationship between plate motions and seismic moment tensors and the rates of active deformation in the Mediterranean and Middle East, *Geophys. J. R. astr. Soc. Lond.*, **83**, 45–73.
- Jackson, J., Haines, J. & Holt, W., 1995. The accommodation of Arabia-Eurasia plate convergence in Iran, *J. geophys. Res.*, **100**, 15 205–15 219.
- King, R.W. & Bock, Y., 2002. *Documentation for the GAMIT analysis software*, release 10.1, Massachusetts Institute of Technology, Cambridge, Massachusetts.
- Maggi, A., Jackson, J.A., Priestley, K. & Baker, C., 2000. A re-assessment of focal depth distributions in Southern Iran, the Tien Shan and Northern India: do earthquakes really occur in the continental mantle?, *Geophys. J. Int.*, **143**, 629–661.
- Masson, F., Chéry, J., Hatzfeld, D., Martinod, J., Vernant, P., Tavakoli, F. & Ghafory-Ashtiani, M., 2005. Seismic versus aseismic deformation in Iran inferred from earthquakes and geodetic data, *Geophys. J. Int.*, **160**, 217–226.
- McClusky, S. et al., 2000. Global Positioning System constraints on plate kinematics and dynamics in the eastern Mediterranean and Caucasus, *J. geophys. Res.*, **105**, 5695–5719.
- McClusky, S., Reilinger, R., Mahmoud, S., Ben Sari, D. & Tealeb, A., 2003. GPS constraints on Africa (Nubia) and Arabia Plate motions, *Geophys. J. Int.*, **155**, 126–138.
- McQuarrie, N., 2004. Crustal scale geometry of the Zagros fold-thrust belt, Iran, *J. Struct. Geol.*, **26**, 519–535.
- Molinaro, M., Zeyen, H. & Laurencin, X., 2005. Lithospheric structure underneath the south-eastern Zagros Mountains, Iran: recent slab break-off?, *TerraNova*, **17**, 1–6.
- Nilforoushan, F. et al., 2003. GPS network monitors the Arabia-Eurasia collision deformation in Iran, *J. of Geodesy*, **77**, 411–422.
- North, R.G., 1974. Seismic slip rates in the Mediterranean and the Middle East, *Nature*, **252**, 560–563.
- Ricou, L.E., Braud, J. & Brunn, J.H., 1977. Le Zagros, *Mém. H. Sér. Soc. Géol. Fr.*, **8**, 33–52.
- Savage, J. & Burford, R., 1973. Geodetic determination of relative plate motion in Central California, *J. geophys. Res.*, **95**, 4873–4879.
- Sella, G.F., Dixon, T.H. & Mao, A., 2002. REVEL: a model for recent plate velocities from space geodesy, *J. geophys. Res.*, **107**(B4), ETG 11-1, 11–32.
- Sherkaty, S. & Letouzey, J., 2004. Variation of structural style and basin evolution in the central Zagros (Izeh zone and Dezful Embayment), Iran, *Marine and Petroleum Geology*, **21**(5), p. 535.
- Shearman, D.J., 1976. Geological evolution of Southern Iran – report of Iranian Makran Expedition, *Geographical Journal*, **142**, 393–410.
- Stocklin, J., 1974. Possible ancient continental margin in Iran, in *Geology of Continental Margins*, pp. 873–877, eds Burke, C. & Drake, C., Springer-Verlag, New York.
- Stoneley, R., 1981. The geology of the Kuh-e-Dalneshin area of southern Iran, and its bearings on the evolution of southern Tethys, *J. geol. Soc. Lond.*, **138**, 509–526.
- Talebian, M. & Jackson, J., 2002. Offset on the main recent fault of the NW Iran and implications on the late Cenozoic tectonics of the Arabia-Eurasia collision zone, *Geophys. J. Int.*, **150**, 422–439.
- Talebian, M. & Jackson, J., 2004. A reappraisal of earthquake focal mechanisms and active shortening in the Zagros mountains of Iran, *Geophys. J. Int.*, **156**, 506–526.
- Tatar, M., Hatzfeld, D., Martinod, J., Walpersdorf, A., Ghafory-Ashtiany, M. & Chéry, J., 2002. The present-day deformation of the central Zagros from GPS measurements, *Geophys. Res. Lett.*, **29**(19), 1927.
- Tatar, M., Hatzfeld, D. & Ghafory-Ashtiany, M., 2004. Tectonics of the Central Zagros (Iran) deduced from microearthquake seismicity, *Geophys. J. Int.*, **156**, 255–266.
- Tchalenko, J.S. & Braud, J., 1974. Seismicity and structure of the Zagros (Iran)—the Main Recent Fault between 33 and 35°N, *Phil. Trans. Roy. Soc. Lond.*, **277**, 1–25.
- Vernant, P. et al., 2004. Present-day crustal deformation and plate kinematics in the Middle East constrained by GPS measurements in Iran and northern Oman, *Geophys. J. Int.*, **157**, 381–398.
- Vita-Finzi, C., 1987. 14C deformation chronologies in coastal Iran, Greece and Jordan, *J. geol. Soc. Lond.*, **144**, 553–560.